1   # Predicting East African spring droughts using Pacific and Indian Ocean
2   # sea surface temperature indices

3   Chris Funk, US Geological Survey and University of California Santa Barbara Geography

4   Andrew Hoell, University of California Santa Barbara Geography

5   Shraddhanand Shukla, University of California Santa Barbara Geography

6   Ileana Blade Mendoza, Universitat de Barcelona and Institut Català de Ciències del Clima

7   Brant Liebmann, University of Colorado and NOAA Earth Systems Research Laboratory

8   Jason B. Roberts, NASA Marshall Space Flight Center

9   Franklin R. Robertson, NASA Marshall Space Flight Center

10 Gregory Husak, University of California Santa Barbara Geography

11

12 **Abstract:**

13 In eastern East Africa (the southern Ethiopia, Eastern Kenya and southern Somalia region), poor

14 boreal spring (long wet season) rains in 1999, 2000, 2004, 2007, 2008, 2009, and 2011

15 contributed to severe food insecurity and high levels of malnutrition. Predicting rainfall deficits

16 in this region on seasonal and decadal time frames can help decision makers implement disaster

17 risk reduction measures while guiding climate-smart adaptation and agricultural development.

18 Building on recent research that links more frequent East African droughts to a stronger Walker

19 Circulation, resulting from warming in the Indo-Pacific warm pool and an increased east-to-west

20 sea surface temperature (SST) gradient in the western Pacific, we show that the two dominant

21 modes of East African boreal spring rainfall variability are tied to SST fluctuations in the

22 western-central Pacific and central Indian Ocean, respectively. Variations in these two rainfall

23 modes can thus be predicted using two SST indices – the West Pacific Gradient (WPG) and

24 Central Indian Ocean index (CIO), with our statistical forecasts exhibiting reasonable cross-

25 validated skill ($r_{cv} \approx 0.6$). In contrast, the current generation of coupled forecast models show no

26   skill during the long rains. Our SST indices also appear to capture most of the major recent

27   drought events such as 2000, 2009 and 2011. Predictions based on these simple indices can be

28   used to support regional forecasting efforts and combined with more sophisticated coupled

29   modeling systems and land surface data assimilations to help inform early warning and guide

30   climate outlooks.

31   **1.   Introduction**

32   **1.1 How understanding trends can lead to better drought predictions**

33   Since 2003, scientists from the University of California, Santa Barbara's Climate Hazards

34   Group, the U.S. Geological Survey, the Universitat de Barcelona, the National Ocean and

35   Atmospheric Administration's (NOAA) Earth System Research Laboratory, Physical Science

36   Division, Climate Analysis Branch, and the National Aeronautics and Space Agency have been

37   working to improve the US Agency for International Development's Famine Early Warning

38   System Network's (FEWS NET) drought early warning capabilities for Eastern Africa. In this

39   introduction, we describe how our deepening understanding of boreal spring rainfall trends can

40   lead to useful new SST indices that support better drought prediction.

41   Early FEWS NET research focused on developing better Ethiopian rainfall archives and

42   historical time series, which revealed substantial 1980-2004 rainfall declines in key crop growing

43   areas in the southern half of the country (Funk et al., 2003). Further diagnostic analysis of sea

44   surface temperatures (SST) and precipitation (Verdin et al., 2005;Funk et al., 2008;Hoell and

45   Funk, 2013a, b;Lyon and DeWitt, 2012;Williams and Funk, 2011) suggested that the recent

46   appearance of more very warm areas (>29°C) in the south-central Indian Ocean and equatorial

47   western Pacific has led to an increase in local precipitation over the ocean but reduced rainfall

48 over Eastern Africa via a Rossby wave-like (Gill, 1980) atmospheric response. One study (Funk

49 et al., 2008) examined the canonical correlation between moisture transports over Eastern Africa

50 and reanalysis precipitation over the Indian Ocean and found that increased precipitation over the

51 south Central Indian Ocean (CIO, 0-15°S, 60-90°E) is associated with decreased easterly low-

52 level moisture flows into the Horn of Africa. Further confirmation of this relationship was

53 obtained from a simulation using the Community Atmospheric Model (CAM), which suggested

54 that anomalous diabatic heating over the Indian Ocean reduced and reduced onshore moisture

55 transports (Funk et al. 2008).

56   These diagnostic analyses were later extended by using a combined Principal Component

57 Analysis (PCA) based on zonal surface winds, 500 hPa vertical velocities, rainfall and SSTs over

58 the tropical Indo-Pacific Area (IPA) (Williams and Funk, 2011). The leading principal

59 component (PC) was shown to represent a low frequency oceanic warming signal associated

60 with an enhancement of the Indian branch of the Walker circulation and with declining rainfall in

61 Eastern Africa and the central equatorial Pacific. Specifically, figures 7 and 8 of Williams and

62 Funk (2011) identified enhanced low level convergence and increases in convection over the

63 warm pool, subsidence over the eastern Horn, westerly surface zonal wind anomalies over the

64 northern equatorial Indian Ocean, and reductions in total atmospheric precipitable water over

65 Eastern Africa.

66   While the 1st mode of Williams and Funk's (2011) combined PCA exhibited a strong secular

67 trend and tracked closely with global average temperatures (r=0.86), the 2nd mode varied on

68 interannual time scales and was strongly related to the El Niño-Southern Oscillation (ENSO),

69 with a negative correlation of -0.75 between its time series and the Niño 4 SST index (5°S-5°N,

70   160°E-150°W). Like the IPA PC1 'trend mode', the 2nd mode (in one of its phases) was

71   associated with drying over East Africa via anomalies in the Indian Ocean Walker circulation

72   The IPA PC1, which was linked to warming in the Indo-Pacific warm pool, appeared to be

73   associated with East African drought in two ways. First, PC1 helps explain the downward 1980-

74   2009 rainfall trends across the eastern portions of the Greater Horn of Africa. Second, it was

75   hypothesized that the enhanced subsidence associated with the increasing PC1 mode would be

76   even stronger when occurring in combination with a La Niña event. Indeed, La Niña events also

77   produce increased upward motion over the equatorial Indo-Pacific and increased subsidence and

78   higher surface pressures over East Africa (Nicholson and Kim, 1997;Nicholson and Selato,

79   2000;Ogallo, 1988). To test this hypothesis, 1950-2009 La Niña events were categorized into

80   warm Warm Pool and cool Warm Pool groups (based on the IPA PC1) and composited.

81   Composites of La Niña events displayed a much stronger negative precipitation anomaly over

82   Eastern Africa when the Warm Pool was warmer. Since the Warm Pool has exhibited a strong

83   increase in temperature over the past few decades, this corresponded with a stronger La Niña

84   teleconnection in the recent period (Williams and Funk, 2011). In particular, over eastern East

85   Africa composites of low PC1/La Niña events had standardized precipitation index (SPI)

86   (McKee et al., 1993) values of about -0.1, while composites of high PC1/La Niña events had SPI

87   values ranging from -0.4 to -0.8. In the summer of 2010, when our NOAA partners predicted that

88   there was a high probability for the development of a strong La Niña, FEWS NET used

89   composites of high PC1/La Niña events to provide early warning of the devastating 2011 drought

90   (Ververs, 2011).

91   In 2012, new research (Lyon and DeWitt, 2012) suggested that a 1998 shift in Pacific SSTs

92   had played an important role in increasing the intensity of the Walker circulation, thereby drying

eastern East Africa. In that study several sets of atmospheric general circulation model (GCM)

simulations were run to isolate the Indian and Pacific effects. Indian Ocean forcing produced

anomalous circulations similar to those identified in prior FEWS NET analyses of Indian Ocean

influences (Funk et al., 2008;Funk et al., 2005;Jury and Funk, 2013;Verdin et al., 2005;Williams

et al., 2011). The Pacific Ocean forcing effects were consistent with those identified in the IPA

analysis of Williams and Funk (2011).

In 2013 and 2014, FEWS NET scientists built on Williams and Funk (2011) and Lyon and

DeWitt (2012) to better explain these teleconnections. Hoell and Funk (2013a) showed that a

stronger West Pacific SST Gradient (WPG) combined with La Niña conditions produced

stronger East African drying. Hoell and Funk (2013a) defined the WPG as the difference

between standardized SST in the Niño 4 region (160°E-150°W, 5°S-5°N) and the western Pacific

(WP, 130-150°E, 0-20°N). Because the standard deviation of WP SST is substantially less than

Niño 4 SST (0.35°C versus 0.7°C) a one degree WP anomaly will have a greater influence on the

WPG index. The physical justification for this is the greater dynamic response associated with

very warm WP SSTs (Folkins and Braun, 2003).

The WPG analysis of Hoell and Funk (2013a) is similar to Williams and Funk (2011), but

offers a more transparent physical mechanism: a strong WPG combined with a cold eastern

Pacific produces a strong SST gradient spanning the entire Pacific basin; stronger SST gradients

are known to produce larger circulation changes (Lindzen and Nigam, 1987). The temporal

response of the WPG combines the long term warming trend of the WP (Funk, 2012) with the

strong ENSO-related variations of the Niño 4 regions.

Recent analyses of atmospheric climate model simulations (Funk et al., 2013;Liebmann et

al., 2014) have shown the link between the WPG and low east African rainfall. Here we explore

5

116   the utility of this index as a basis for predicting the first principal component of East African

117   boreal spring precipitation. Recent assessments (Nicholson, 2014a) have examined multivariate

118   predictions of East African long rains; our objective here is not to replicate this work, but rather

119   to examine forecasts based on indices linked to our process-based studies of the effects of

120   stronger Pacific SST gradients. Since global climate models have almost no skill forecasting the

121   long rains (Mwangi et al., 2014), the modest cross-validated skills we find here is still likely to

122   be useful.

123   The WPG and CIO indices, furthermore, can link the process-based studies discussed above

124   with the requirements of real time monitoring and climate diagnostics and analyses. Such

125   analysis helped FEWS NET identify analog years and effectively communicate risks to decision

126   makers in 2011 (Ververs, 2011) and 2012 (US, 2012). Our main point is that there are important

127   climate indices, beyond the well-known Niño 3.4 (Indeje et al., 2000) and the Indian Ocean

128   Dipole (IOD) indices (Saji et al., 1999), that can inform East African climate outlooks such as

129   the Greater Horn of Africa Climate Outlook Fora. While these other indices are good indicators

130   of the region's boreal fall 'short' rains, the WPG may be preferable during boreal spring because

131   of the high sensitivity this season exhibits to WP and Niño 4 SST.

132   **1.2 Climate change and Pacific decadal variability (PDV)**

133   Long rain declines have been confirmed by many recent studies (Funk et al., 2012;Liebmann

134   et al., 2014;Lyon and DeWitt, 2012;Viste et al., 2012), and corroborated by analyses of

135   Normalized Difference Vegetation Index imagery (Pricope et al., 2013) and satellite observed

136   soil moisture (Omondi et al., 2013). Omondi et al. (2013) identify a large post-2005 decline in

137   Gravity Recovery and Climate Experiment (GRACE) soil moisture values over the Greater

138   Horn. These declines appear consistent with the detailed 2008-2011 drought analyses provided

139   by Nicholson (Nicholson, 2014b). The source of the SST forcing behind recent East African

140   rainfall declines, however, continues to be a matter of considerable debate.

141   One interpretation (Funk et al., 2013) is that the recent strengthening of the WPG, Warm

142   Pool precipitation increases, and related East African precipitation declines, is a function of

143   anthropogenic warming in the WP combined with natural decadal cooling in the central Pacific.

144   Both the WP SST (Hoell and Funk, 2013b) and the WPG (Hoell and Funk, 2013a) have

145   increased dramatically over the past thirty years, increasing the frequency of droughts and the

146   number of opportunities for drought prediction. Hoell and Funk (2013b) compare the influence

147   of WP, IOD and ENSO influences on boreal spring East African rainfall, and find that WP

148   drought influences tend be as strong as or stronger than IOD and ENSO. This view implies that

149   WP warming is largely anthropogenic and has contributed to recent East African drying.

150   An alternative interpretation (Lyon et al., 2013;Yang et al., 2014) suggests that the dominant

151   driver of recent East African has been PDV, interpreted as linearly detrended ENSO-residual

152   changes in Pacific SST. Lyon et al. (2013) make a convincing and important case for the large

153   dynamic response associated with the tropical SST anomaly pattern found in detrended ENSO-

154   residual SST. The research presented in Lyon and DeWitt (2012), furthermore, helped motivate

155   the gradient analyses leading to this current publication. The research presented here, however,

156   suggests that i) most of the recent 'decadal' variability in detrended western Pacific SST arises

157   due to anthropogenic warming, so that ii) decadal East African long rains variability can best be

158   described by a combination of a recent secular decline and decadal variations. We furthermore

159   (iii) suggest that an understanding of the greater sensitivity of East African precipitation to WP

160   versus Niño 4 warming may help support more effective precipitation forecasts.

161   **1.3 Paper organization**

162   This paper is organized as follows. Section 2 describes our datasets. Section 3.1 describes our

163   two prediction targets: the first and second principal components (PC1 and PC2) of East African

164   precipitation for the 1981-2013 time period, estimated using the new 0.05°x0.05° gridded

165   Climate Hazards group Infrared Precipitation with Stations (CHIRPS) data (Funk et al., 2014).

166   We first briefly describe the CHIRPS precipitation dataset; then we explore the pattern and time

167   series associated with the first two principal components during the March-May season. Spatial

168   correlations (Section 3.2) between these principal components and antecedent (January) SST

169   show that the leading spatial pattern (PC1) exhibits Pacific SST gradients similar to the WPG

170   (Hoell and Funk, 2013a) and correlation structures between East African precipitation and SSTs

171   (Funk et al., 2013;Liebmann et al., 2014;Tierney et al., 2013). The second mode SST correlation

172   structure (PC2), on the other hand, is similar to the patterns found in earlier studies (Funk et al.,

173   2008;Funk et al., 2005) focused on the CIO. In Section 3.3 we show that the WPG and CIO

174   indices can be useful large scale climate indicators when used to predict PC1 and PC2. We relate

175   PC1 to the WPG, and PC2 to CIO SST. We then show that these simple indices provide a

176   reasonable basis for forecasting some East Africa precipitation extremes. Section 3.4 provides a

177   case study forecasting the 2014 long rains. Section 3.5 provides a brief analysis of long term

178   changes in WPG SSTs in both observations and model simulations. Section 4 summarizes our

179   results.

180   **2. Data**

181   This study focuses mainly on the relationships between CHIRPS March-May rainfall over a

182   region extending across the southern Arabian peninsula and eastern East Africa (25°E-55°E,

183   13°S-20°N) and January NOAA Extended Reconstruction version 3b SST (ER3b) (Smith et al.,

184   2008). The CHIRPS study precipitation region was selected based on i) the climatological

185 importance of March-May rainfall, ii) a known sensitivity to Indo-Pacific forcing and iii) high

186 underlying levels of food and water insecurity. The study focuses on Yemen, Djibouti, Eritrea,

187 Ethiopia, Somalia, Kenya, and Tanzania.

188 The 1981-2013 CHIRPS data set (Funk et al., 2014) combines satellite cold cloud duration

189 rainfall estimates with gauge observations and a high resolution (0.05°) precipitation

190 climatology. Comparisons between the CHIRPS fields and two state-of-the-science data sets: the

191 Global Precipitation Climatology Centre data set (Schneider et al., 2013) and the Global

192 Precipitation Climatology Project (Adler et al., 2003) data sets, reveal a reasonable level of

193 correspondence among all three data sources. We compare the major modes of variability

194 (principal components) of the March-May CHIRPS with January SSTs from the Extended

195 Reconstruction version 3b SST (ER3b) (Smith et al., 2008).

196 The final section of the analysis presented here considers a longer time span (1920-2013)

197 using the gridded Global Precipitation Climatology Centre (GPCC) dataset. The analysis was not

198 pushed further back in time because of concerns about the limited and poor quality East African

199 station data (Liebmann et al., 2013). This final section also uses an ensemble of 53 Phase 5

200 Coupled Model Intercomparison Project (CMIP5) simulations from 14 models (Taylor et al.,

201 2011). In these runs, coupled atmosphere-ocean general circulation models are initialized,

202 allowed to spin up for several hundred years, and then used to simulate climate from 1850

203 onward. The models are driven by observed changes in greenhouse gasses, solar insolation and

204 aerosols. The models used are listed in Table 1. These CMIP5 simulations were obtained from

205 the Royal Netherlands Meteorological Institute's Climate Explorer.

206 **3. Results**

207 **3.1 CHIRPS principal component patterns and time series**

9

208   Principal component analysis (PCA) provides a way of compactly summarizing the spatio-

209   temporal variations in data sets. PCA produces matched sets of principal component time series

210   and spatial patterns (loading maps, based on the covariance matrix). The first principal

211   component time series and associated pattern describes the largest possible amount of the

212   variance by aggregating locations that tend to be positively or negatively correlated with each

213   other. At a given time step, multiplying the PC1 time series value by the associated first

214   principal component loading map produces the partial contribution of that PC to total rainfall.

215   This process can be repeated for the second component, which explains most of the remaining

216   variance of the data, after the first principal component has been removed. We will predict the

217   leading two March-May PC1 and PC2 time series using January WPG and CIO SST indices and

218   then use these two components to generate March-May rainfall prediction maps. The January

219   SST data was chosen as a predictor because the East African climate experts typically gather in

220   mid-February at the Greater Horn of Africa Climate Outlook Forum (GHACOF) to produce a

221   regional forecast for East Africa. PCA provides an alternative to the definition, analysis and

222   prediction of homogeneous rainfall areas (cf. Nicholson 2014a). For most forecasting

223   applications, analysis of homogeneous areas is preferable. We have used PCA values in this

224   illustrative study because they provide, by definition, representative time series that describe the

225   highest possible precipitation variance. They therefore provide insight into regional

226   precipitation-SST relationships, and can help benchmark forecast relationships used in regional

227   land surface models as in Shukla et al. (2014ab).

228   Figure 1 shows the first and second principal component maps and time series for our

229   extended East African region. The principal components were calculated based on the 1981-2013

230   covariance matrix. PC1 and PC2 explained 26% and 12%, respectively, of the total rainfall

231 variance in the study region. Experiments with different spatial domains indicated very little

232 (substantial) sensitivity to variations in the north-south (east-west) limit and size of domain,

233 especially for PC1. This sensitivity, and the temporal loading patterns of PC1, indicate that we

234 are primarily focusing on the eastern East Africa region identified as a homogenous area by

235 Nicholson (2014a) and Liebmann et al. (2014).

236   Figures 1a and 1b show the changes in standardized precipitation associated with PC1 and

237 PC2. The spatial loading patterns have been scaled by the 1981-2013 trends in PC1 and PC2, and

238 then divided by the standard deviation of rainfall at each location. This provides an estimate of

239 the 33-year change in the standardized precipitation associated with the first and second mode.

240 The linear trend in PC1 is significant (p=0.03), the trend in PC2 is not (p=0.11).

241   This can help us understand the contributions of changes in the first and second principal

242 components to the total observed trends (shown in Fig. 1c). Standardized changes are shown to

243 shown to emphasize the emergent food security risks in the red areas of Fig. 1c. In these regions

244 rainfall has decline by more than half a standard deviation, greatly increasing the frequency of

245 below normal crop and pasture conditions.

246   Figure 1a indicates substantial rainfall declines associated with PC1, extending from northern

247 Tanzania through Yemen, with the strongest standardized declines being found just north of the

248 equator, but with large declines (more than half a standard deviation) occurring in a large part of

249 the domain. Figure 1b was created in an identical fashion, using PC2. This pattern tends to

250 emphasize off-equatorial regions of Tanzania, northern Ethiopia, Eritrea, and Djibouti, but PC2

251 does not appear to have contributed substantially to recent rainfall declines. Figure 1d shows the

252 time series for these two principal components. Figures 1e and 1f show the rainfall loading

253 patterns associated with PC1 and PC2. The first principal component identifies many intense

254   drought years: 1984, 1992, 1999, 2000, 2004, 2008, 2009, and 2011. The large negative PC2

255   values in 1988, 2003, 2008, 2009, and 2013 were associated with dryness in Tanzania and

256   Ethiopia, but not near the equator. Both time series exhibit substantial interannual variations.

257   PC1 indicates substantial declines between 1981 and 2013.

258   The total rainfall trend for this period is presented in Fig. 1c. This trend pattern suggests that

259   the substantial rainfall declines that have occurred during the last 20 years (1994-2013) can be

260   ascribed largely to the first leading mode. We next examine the relationships between the

261   corresponding time series and antecedent January SST. Analysis of January SST can inform

262   regional food security outlooks, providing sufficient lead time to shape contingency plans, guide

263   resource distribution, and help pre-position humanitarian assistance *before* long rainy season

264   droughts begin.

265   **3.2 Correlations with January SST**

266   The correlation results presented here (Fig. 2a) use a 1994-2013 period because the studies

267   discussed above (Funk et al., 2008;Hoell and Funk, 2013a, b;Lyon and DeWitt, 2012;Verdin et

268   al., 2005;Williams and Funk, 2011) indicate a recent increase in the sensitivity of East African

269   precipitation to Indo-Pacific SST forcing. This increase in sensitivity is likely related to the long

270   term WP warming trend (Williams and Funk, 2011; Hoell and Funk, 2013b), an increase in the

271   Indian branch of the Walker circulation (Williams and Funk, 2011; Liebmann et al. 2014), and a

272   stronger WPG (Hoell and Funk, 2013a). Changes in these climate conditions accompanied by a

273   future transition to a warmer central Pacific (as predicted by climate change models) might

274   weaken the boreal spring teleconnection pattern.

275   It should be noted that the strength of these SST correlations depend on the time period

276   analyzed. As discussed in Funk et al. (2013) or Liebmann et al. (2014), the strong negative

277   correlation structure shown in Fig. 2a has only manifested since the mid-1990s. Running

278   correlations with Niño 3.4 SSTs indicate weak relationships before that period (Funk et al.

279   2013). Analysis of 1948-1987 climate data (Hastenrath et al., 2011), furthermore, indicate weak

280   teleconnections between Kenyan boreal spring rainfall and the atmospheric circulation over the

281   Indian Ocean. As the mean Walker Circulation has intensified (L'Heureux et al., 2013),

282   however, the East African drought impacts of La Niña-like SST patterns has intensified

283   (Williams and Funk, 2011) due to the influence of a stronger WPG (Hoell and Funk, 2013a),

284   resulting in the type of correlation structure shown in Fig. 2a. Atmospheric Global Circulation

285   Models (AGCMs) have also been used to confirm the plausibility of this correlation pattern

286   (Hoell and Funk, 2013b; Liebmann et al., 2014; Lyon and DeWitt, 2012).

287   The correlations (Fig. 2a) between the March-May PC1 (solid red line, Fig. 1d) and the

288   preceding January SST field indicate that a stronger than normal west-to-east warm-to-cool

289   Pacific SST gradient over the tropical Pacific is associated with dry conditions over most of the

290   Horn of Africa, consistent with earlier findings (Tierney et al., 2013;Lyon and DeWitt,

291   2012;Liebmann et al., 2013;Hoell et al., 2013;Hoell and Funk, 2013c;Hoell and Funk,

292   2013d;Hoell and Funk, 2013e;Funk et al., 2013). The blue and red boxes denote the Niño 4 and

293   WP regions; the WPG index is estimated as the SST difference between these regions following

294   Hoell and Funk (2013b).

295   The correlation pattern associated with PC2 (Fig. 2b) identifies warming in the Indian Ocean

296   with drying in parts of the Horn of Africa, particularly Ethiopia and Tanzania. These results are

297   also consistent with prior research focusing on the causes of Ethiopian rainfall declines, which

298 identified teleconnections to the Indian Ocean (Williams et al., 2011;Funk et al., 2005;Jury,

299 2010). While other regions in Fig. 2b exhibit significant correlations, we focus here on the CIO

300 because of prior literature and the plausible physical teleconnection between this region and the

301 adjacent Greater Horn of Africa. Nonetheless, warming in the central Pacific also appears to be

302 associated with East African drying (in contrast to the pattern associated with PC1).

3.3 Using January WPG and CIO indices to predict March-May CHIRPS PC1 and PC2

304   Two regression prediction time periods for the PC1 time series were compared: 1981-1993

305 (Fig. 3a) and 1994-2013 (Fig. 3a). The PC1 variance explained by the WPG index over the 1994-

306 2013 time period was substantially larger, with the WPG index explaining 50% of the PC1

307 variance as opposed to 0% over the 1981-1993 time period. Over the 1994-2013 time period, the

308 regression slope between the March-May CHIRPS PC1 and the January WPG index indicates a

309 modest negative relationship (not shown), with a one standard deviation decrease in the WPG

310 (designating a stronger Niño4 to WP gradient) being associated with a 0.5 standardized deviation

311 decrease in PC1. In this study, which focuses on developing a framework to anticipate the next

312 drought, we use the regression coefficients from the shorter time period to estimate rainfall

313 associated with PC1 based on the western Pacific SST gradient index (WPG), while emphasizing

314 the need to monitor the stationarity of the La Niña-East Africa teleconnection. The strength of

315 this modest teleconnection is quite similar to results obtained from ECHAM5 simulations

316 (Liebmann et al., 2013).

317   For the PC2 time series, we used a regression based on the full period of record (1981-2013),

318 since the negative relationship between SST in the CIO region (0-15°S, 60-90°E) and PC2 was

319 found to be robust throughout the time period evaluated. The corresponding 1981-2013

14

320   regression explained 33% of the total variance of PC2. For every standard deviation increase in

321   CIO SSTs, PC2 declined -0.6 standard deviations.

322   The two leading CHIRPS principal components during March-May over East Africa relate,

323   respectively, to SST anomalies in the Pacific and Indian Oceans (Fig. 2) during January. Figure

324   3a-c show scatter plots of the cross-validated 1994-2013 PC1, 1981-1993 PC1 and 1981-2013

325   PC2 estimates. The cross-validation was carried out using a 'leave-one-out' algorithm. Each

326   year's data was withheld, the regression coefficients re-estimated and the regression estimate for

327   the withheld year compared to the corresponding observed data. The y-axes depict the observed

328   March-May principal components from the CHIRPS data. The time series of these components

329   are also plotted in Fig. 1d. The x-axes represent jack-knifed regression estimates of these PCs

330   based on either the WPG or CIO indices calculated from January SST. Over the past twenty

331   years, the combination of wintertime La Niña conditions and warm western Pacific SSTs (large

332   WPG) presage low PC1 values (Fig. 3a). The three most extreme dry (low PC1) seasons in this

333   period (1999, 2000 and 2011) are captured well (dark black diamonds). Over the 1981-1993

334   period, the PC1 WPG relationship was weak (Fig. 3b), consistent with the aforementioned

335   reports of a weak zonal connections in the Indo-Pacific (Hastenrath et al., 2011). The skill of the

336   CIO index, on the other hand, comes more from distinguishing between high PC2 values

337   associated with relatively cool Indian Ocean SSTs between 1981 and 1996 and low PC2 values

338   related to the warm Indian Ocean conditions that have persisted since 1997. These time periods

339   are denoted respectively, with diamonds and triangles in Fig. 3c.

340   These simple WPG and CIO indices can thus be used to predict PC1 and PC2, which can

341   then be multiplied against their loading maps and summed to produce hindcasts of East African

342   March-May rainfall. The correlation between these forecasts and observed 1994-2013 CHIRPS

343   rainfall is shown in Fig. 3d. The eastern Horn of Africa, southern Tanzania, Eritrea, Djibouti, and

344   Yemen all exhibit positive correlations. One region of northern Tanzania is poorly represented,

345   and exhibits negative correlations. While rainfall in northern Tanzania has been declining (Fig.

346   1c), these declines seem poorly related to WPG/PC1 or CIO/PC2 changes. Regional climate

347   change simulations (Cook and Vizy, 2013) have suggested that this region may be more sensitive

348   to changes in trans-Congo moisture transports, while drying in Kenya, southern Somalia and

349   southern Ethiopia might be related to changes in the Somali Jet.

350   Figure 4 shows forecast and observed rainfall anomaly maps for a selection of dry and wet

351   seasons. While the index-based forecasts tend to under-estimate the variance of the rainfall, the

352   ability to discriminate between wet and dry seasons at a regional scale seems promising.

353   Likewise, although the ability to discriminate between normal and above normal PC1 values

354   seems limited (Fig. 3a), extreme dry years appear to be fairly well predicted. Thus our index-

355   based predictions can capture some of the extreme drought years (2000, 2009, 2011), but do not

356   predict well some above normal wet seasons (such as 2006 and 2013). SST composites of wet,

357   normal, and dry seasons (not shown) indicate a much more well-defined structure during dry

358   seasons, with most dry years being associated with a strong WPG. Between 1994 and 2013,

359   strong WPG events have been associated with observed rainfall ranging from normal to far

360   below normal (Fig. 3a). When WPG conditions are neutral or indicative of El Niño-like

361   conditions, the relationship between WPG and EA long rains seems quite weak (Fig. 3a).

362   We hypothesize that there may be a nonlinear East African precipitation response to WP and

363   Niño 4 SST variations caused by the interaction of the long term warming trend and ENSO. Over

364   the past twenty years, during La Niña events, the effects of the long term WP warming trend and

365   cold Niño 4 SST act to reinforce each other, making droughts more predictable. During neutral

366 or El Niño-like conditions, instead, the two effects cancel out and East African precipitation may

367 be more influenced by less predictable Indian Ocean SST, variations in the Madden-Julien

368 Oscillation (Pohl and Camberlin, 2006), or internal atmospheric dynamics. Absent the combined

369 influences of warm WP and La Niña conditions, these natural weather variations may play a

370 more dominant role in producing normal or above normal East African precipitation.

371 **3.4 A case study addressing the 2014 long rains**

372 Here we briefly describe how the WPG and CIO indices were used in February of 2014 to

373 produce an operational forecast for FEWS NET. This case study provides an example of how

374 these indices might be used in the context of a GHACOF forecast setting. Despite weak forecasts

375 for the onset of El Niño conditions, the ocean in January of 2014 exhibited substantial warm

376 (cold) conditions in the WP (Niño 4) region, indicating a strong WPG (Fig. 5a). CIO conditions

377 (Fig. 5a) were close to neutral, or slightly warm. Given that the regression between 1994-2013

378 East African March-May standardized precipitation index and January WPG indicates reasonable

379 levels of skill (r=0.57) and is able to identify the worst drought years (recall section 3.3), this

380 regression was used to produce a forecast for modestly below normal rainfall (X in Fig. 5b). This

381 forecast and the assumption of gaussianity was used to derive tercile-based probability forecasts,

382 indicating normal to below normal rains (Fig. 5c).

383   While no forecast methodology should be validated based on a single season, the FEWS

384 NET prediction made in February of 2014 proved to be reasonably accurate. Strong Pacific

385 gradient (WPG) conditions persisted into April and May. While March 2014 rains were above

386 normal, April and May totals were very low over much of Kenya and Southern Ethiopia (Fig.

387 5d), with rainfall rank imagery indicating rains in the bottom five years of the 1981-2014

388 CHIRPS archive. Time series of Kenyan/Southern Ethiopian April-May rainfall from the GPCC

389   and CHIRPS archives (Fig. 5e) place this dry season in deeper historical context. The region

390   used in the areal averages (shown as the red polygon in the inset on Fig. 5e) covers all Kenya

391   except Western and Nyanza province, south-central and south-eastern Ethiopia. In this region 16

392   of the 24 April-May seasons since 1991 (66%) have received less than 190 mm of rainfall, the

393   1930-1980 average. We therefore conclude that at least some of the most extreme dry seasons

394   seem to be predictable and associated with strong WPG conditions.

395   **3.5 Examining long time series of East African rainfall and SSTs**

396   We briefly examine long time series of East African rainfall and SSTs. Our objective is to place

397   recent East African rainfall declines in a deeper historic context. We have averaged the GPCC

398   interpolated gauge dataset over our entire study region (25°E-55°E, 13°S-20°N), converted the

399   resulting time series into an EA SPI time series (McKee et al., 1993), smoothed the results with

400   ten year running means, and plotted the results in Fig. 6a. Between 1920 and 1980, the GPCC

401   time series exhibits substantial inter-decadal oscillations (Lyon et al., 2013;Lyon and DeWitt,

402   2012;Yang et al., 2014), indicative of the climate sensitivity of this semi-arid region. After 1980,

403   the GPCC begins a large decline to arrive at a very low decadal average SPI of -0.7. We have

404   used a regression based on 1930-2012 January WP and Niño 4 SST data to create standardized

405   estimates of the WPG time series. This gives us a way to quantify the relative influence of WP

406   and Niño 4 SST changes. The results indicate an almost one to one correspondence between WP

407   SST changes and the East African SPI time series: one degree of WP warming is associated with

408   about one standardized anomaly decrease in rainfall (b_{WP} = -0.997). The sensitivity to Niño 4

409   SST changes is substantially less and of the opposite sign. One degree of Niño 4 warming is

410   associated with about a +0.4 standardized anomaly increase in rainfall (b_{N4} = +0.419). These

411   results seem plausible given the very warm average SST found in the Warm Pool (~29°C).

18

412 Relatively small increases in temperatures in the Warm Pool are associated with relatively large

413 increases in moist entropy and precipitation (Folkins and Braun, 2003). These empirical results

414 suggest that boreal spring EA precipitation exhibits a greater sensitivity to WP warming.

415 These WP and Niño 4 slope parameters can be used to estimate EA SPI as shown in Fig. 6a

416 (r=0.55, p=0.05, based on 7 d.o.f.). Note that while these estimates fail to recreate the 1920-1980

417 decadal oscillations, they do capture well the post-1990 GPCC decline. While the EA SPI peaks

418 during the 1930s and 1980s and declines during the 1950s, these changes do not seem well

419 represented by the WP and Niño 4 variations. This suggests that the WP and Niño 4 influences

420 on EA precipitation are *not* strongly modulated by PDV. While deviations around our regression

421 estimates are likely related to PDV (Yang et al., 2014), these PDV contributions have probably

422 not produced, alone, the observed -0.7 decline in the GPCC SPI time series (Fig. 6a).

423 We can make this case more explicitly by examining in Fig. 6b the individual WP and

424 NINO4 time series contributions to the regression estimate shown in Fig. 6a. Contributions based

425 on the observed WP and Niño 4 time series are shown along with estimated contributions based

426 on the CMIP5 ensemble means. These time series were produced by multiplying the WP and

427 Niño 4 SST time series by the regression coefficients used in Fig. 6a ($b_{WP} = -0.997$, $b_{N4} =$

428 +0.419). What this decomposition (Fig. 6b) suggests is that between the 1920s and 1980s, the

429 modest drying effect of warming in the WP and the modest wetting effect of warming in the

430 Niño 4 region more or less canceled each other out, resulting in little change in the regression

431 estimates shown in Fig. 6a. Some in the 1990s this may have changed, as the WP warming

432 accelerated, and the high WP sensitivity led to rapid declines in the estimated WP SPI (Fig. 6b).

433 The 1990-2014 SPI increases associated with Niño 4 warming (Fig. 6b) on the other hand, have

434 not kept pace, both because of the lower Niño 4 sensitivity, and because Niño 4 warming has

435   stalled since the beginning of the post-1998 hiatus (England et al., 2014;Meehl et al., 2013).

436   While both the WP and Niño 4 regions have warmed, producing a drying (wetting) effect

437   through the negative (positive) influence of the WP (Niño 4) regions, the overall drying effect of

438   the WP warming (based on our regression) appears to have been greater.

439   We next examine the relationship between WP SST and the effects of radiative forcing, as

440   represented by a CMIP5 ensemble. Fig. 6c shows the smoothed observed WP SST time series

441   and the multi-model ensemble mean WP SST time series from the CMIP5 models listed in Table

442   1. The smoothed time series track closely (r=0.89, p=0.01, based on 7 d.o.f.). Note that there are

443   'decadal' variations in the radiatively forced CMIP5 SSTs. These fluctuations are caused by the

444   warming impacts of greenhouse gases, changes in solar insolation, and the cooling effects of

445   aerosols and volcanic eruptions. Because we have averaged across a large number of

446   simulations, any internal ENSO or PDV signal has been removed. The CMIP5 WP SST

447   increases in 1930s and 1940s, stabilizes in the 1950s, cools for a brief period in the 1960s, and

448   increases at an accelerated rate since about 1980. These decadal fluctuations match reasonably

449   well with changes seen in the observed SST, except for an observed SST increase in the early

450   1950s.

451   It is important to realize that these influences can produce low frequency fluctuations that

452   appear similar to natural 'internal' decadal variations. An example of this is shown in Fig. 6d.

453   Linear fits to the observed and CMIP5 WP SST time series have been removed and the residuals

454   plotted. Because we have averaged across a large number of CMIP simulations (53), any

455   'internal' variations associated with natural climate variability should be greatly diminished in

456   the CMIP ensemble mean time series. Nonetheless, we see large swings in CMIP WP SST that

457   are caused by changes in radiative forcing. Overall, the residuals from a linear fit to the

458 radiatively forced CMIP5 WP ensemble SST (dashed blue line) correspond closely (r=0.69,

459 p=0.04, based on 7 d.o.f.) with the residuals from a linear fit with to the observed data (solid red

460 line). Much of the decadal and longer variation around a linear fit to the WP SST data is likely

461 due to external radiative forcing, especially over the past thirty years. New research has

462 highlighted the important climate impacts associated with the 1st principal component of

463 detrended SST (Lyon et al. 2013); Fig. 6d suggests that these detrended SST are likely to have

464 substantial decadal variations influenced by changes in greenhouse gasses, aerosols and

465 insolation. Western Pacific PDV is largely driven by changes in radiative forcing.

466 **4. Summary**

467 Building on recent diagnostic studies, this paper has explored the utility of two simple SST

468 indices related to the first two principal components of East African spring rainfall. Interestingly,

469 the two principal component modes were found to relate to the WPG and CIO, as identified in

470 prior FEWS NET research focusing on Warm Pool (Hoell and Funk, 2013a, b;Liebmann et al.,

471 2014;Williams and Funk, 2011) and Central Indian Ocean (Funk et al., 2008;Funk et al., 2005)

472 warming. In this study, warming in the WP and cooling in the Niño 4 region was related to

473 rainfall deficits across much of the eastern Horn of Africa (lower PC1 values, Fig. 1d). Warming

474 in the CIO was related to declines in Tanzania and the northeastern Horn (lower PC2 values, Fig.

475 1d). Thus warming in both the western Pacific and Indian Ocean has likely contributed to

476 declines in PC1 and PC2. These SST changes, occurring since the mid-1980s, can be attributed

477 to increases in anthropogenic forcing; the CMIP5 ensemble examined here produced a near-

478 perfect forecast (Fig. 6c) of decadal WP SST variations (r=0.89), and WPG-based regression

479 estimates link this warming (Fig. 6b) with substantial EA precipitation declines. 'Decadal' WP

480 variations, denoted as deviations from a linear trend, are almost completely explained by the

21

481   recent acceleration of anthropogenic warming (Fig. 6d). While PDV certainly influences Niño 4

482   SSTs, contributing to a hiatus (England et al., 2014) in the Niño 4 contribution to EA rainfall

483   shown in Fig. 6b, these influences do not appear to dominate the recent drying tendencies, which

484   appear to be mostly explained by the influence of the western Pacific (Hoell and Funk, 2013b) in

485   a manner consistent with the long (1300-1950) anti-correlation between paleoclimate records of

486   East African precipitation and west Pacific SST (Tierney et al., 2013). An important take home

487   message of the work presented here is that the high sensitivity of East Africa to WP warming

488   presents both a risk and an opportunity. As the warm WP continues to warm we may see more

489   frequent strong gradient events, like the SST conditions during January 2014 (Fig. 5a). Spotting

490   these events, however, requires attention, since they are typically associated with relatively small

491   SST anomalies, since the SST variance in the western Pacific is quite low.

492   Facing the 21st century, we can be fairly sure that the combination of warming air

493   temperatures, growing population, and increasing demands for food will create an enhanced

494   sensitivity to hydrologic extremes in East Africa. At the same time, the large scale climate, both

495   in observations and in CMIP5 models, seems to indicate both a strengthening of the ENSO signal

496   and the ENSO-residual Walker circulation (Sandeep et al., 2014). These tendencies, like the WP

497   and Niño 4 time series shown in Fig. 6b, indicate warming across the Pacific basin. This

498   warming, however, will likely appear sporadically in space and time, likely creating more intense

499   positive or negative SST gradients (cf. Fig. 5a). Taking advantage of the predictability created by

500   these gradients will help us adapt to climate change and our increasing demands for water. While

501   coupled ocean-atmosphere general circulation forecast models provide a valuable resource, we

502   should not expect these systems to always reproduce all the details of climate teleconnections or

503   climate change correctly. The current generation of models struggle to accurately recreate

504   seasonal rainfall variations over East Africa's complex terrain (Mwangi et al., 2014). The simple

505   observationally-based SST indices used here, provide a way of partially overcoming model

506   limitations. More complex statistical models, tailored to East Africa's many diverse climate

507   regions, hybrid statistical-coupled model predictions (Shukla et al. 2014ab) and mesoscale model

508   simulations might all provide potentially better ways to build on the predictive relationships

509   explored here.

510   It should be stressed, however, that statistical relationships can be non-stationary in nature

511   and should be monitored closely. For example, running correlations with March-May NINO3.4

512   SSTs (Funk et al., 2013) show an emerging negative relationship between East African rainfall

513   and Nino3.4 SST. This teleconnection should be routinely monitored, if statistical models such

514   those proposed here are to be used for hydrologic early warning. Conditions that might indicate a

515   weakening of the WPG teleconnection would include climate shifts indicative a weaker Walker

516   circulation: less warm pool precipitation, weaker upper level easterly flows over the Indian

517   Ocean, and weaker easterly trade winds over the central equatorial Pacific Ocean. If the central

518   Pacific suddenly warms dramatically, WPG-induced droughts might become much less frequent.

519   Whatever the future brings, integrated hydrologic early warning systems will help us prepare

520   for extremes. To best address this challenge, multiple sources of information should be

521   combined. Rainfall climatologies, like the CHIRPS, can help us assess historical risks. Just

522   before the onset of rains, appropriate SST indices can guide food security outlooks and

523   GHACOF projections, as illustrated in Section 3.4. The modest levels of skill of these forecasts

524   far exceeds the performance of current generation coupled forecast systems, which show no

525   appreciable skill for the long rains (Mwangi et al., 2014). Coupled models *do*, however, make

526   skillful forecasts over the Indian and Pacific oceans, and these forecasts can be combined with a

23

527   statistical constructed analog (CA) formulation to make skillful predictions of East African

528   rainfall (Shukla et al., 2014a).

529   Once the rainy season begins, land surface conditions becomes an additional source of

530   information – and predictability comes from both the state of the large scale climate and the local

531   antecedent soil moisture conditions (Shukla et al., 2013). Land surface models (LSMs) can add

532   substantial increases in drought prediction skill by incorporating the knowledge of initial

533   hydrologic conditions (derived by forcing the models with observations of rainfall, radiation and

534   air temperature through the time of forecast initialization) in the prediction (Shukla et al., 2013).

535   New hydrologic forecast systems that blend these observations with climate predictions

536   (Sheffield et al., 2013;Shukla et al., 2014b) hold forth exciting new prospects for better early

537   warning. Shukla et al. (2014b) describe a hybrid statistical-coupled model forecast system that

538   uses coupled model Indo-Pacific SST and precipitation forecasts to assign probabilities to past

539   seasons. WPG-like metrics are used to quantify the similarity between current and past climate

540   conditions. These probabilities are then used to sample (bootstrap) the historical LSM forcing

541   archive, preferentially selecting more often years considered similar to the current season. This

542   type of system can incorporate both the observed soil moisture condition and seasonal forecast

543   information, leading to more skillful mid-season predictions. While it seems likely, at least under

544   current negative PDV conditions, that East Africa will continue to face more frequent droughts,

545   rapid advances in prediction systems may help us mitigate their impacts.

546

547

548   Table 1. Coupled ocean-atmosphere models used in this study.

Modeling Group
Commonwealth Scientific and Industrial Research Organization (CSIRO) and Bureau of Meteorology (BOM), Australia
Canadian Centre for Climate Modelling and Analysis
National Center for Atmospheric Research
Community Earth System Model Contributors
Centre National de Recherches Météorologiques / Centre Européen de Recherche et Formation Avancée en Calcul Scientifique
EC-EARTH consortium
The First Institute of Oceanography, SOA, China
NOAA Geophysical Fluid Dynamics Laboratory
NASA Goddard Institute for Space Studies
Met Office Hadley Centre
Institute for Numerical Mathematics
Institut Pierre-Simon Laplace
Atmosphere and Ocean Research Institute (The University of Tokyo), National Institute for Environmental Studies, and Japan Agency for Marine-Earth Science and Technology
Max-Planck-Institut für Meteorologie (Max Planck Institute for Meteorology)

549

550   **Figure Legends**

551   **Figure 1**. **a**. Thirty-three year changes in standardized March-May precipitation associated with the
552   trend in principal component 1 **b**. same for principal component 2. **c**. Thirty- three year changes in
553   standardized March-May precipitation associated with a linear trend **d**. Standardized time series of PC1
554   (solid red line) and PC2 (dashed blue line).

555 **Figure 2. a**. correlations between March-May CHIRPS PC1 and January SSTs **b**. same for CHIRPS PC2.
556 Values have been screened at a 10% significance level. Boxes in panel **a** and **b** show the regions used to
557 the define the WPG and CIO SST indices.

558 **Figure 3**. **a**. Scatterplot of 1994-2013 March-May PC1 observations (y axis) and cross-validated PC1
559 estimates based on January WPG SSTs (x axis). **b**. Same but for 1981-1993. **c**. Scatterplot of 1981-2013
560 March-May PC2 observations (y axis) and PC1 estimates based on January WPG SSTs (x axis). **d**. 1993-
561 2013 correlation between forecasts and observed rainfall.

562 **Figure 4**. Forecasts and observed March-May SPI values for 2000, 2006, 2009, 2010, 2011 and 2013.

563 **Figure 5**. **a**. January 2014 SST anomalies. **b**. Scatterplot of observed and hindcast East African March-
564 May SPI values. Bold diamonds denote 2000, 2009 and 2011. The bold X marks the forecast for 2014
565 made in February of 2014. **c**. Forecast rainfall tercile probabilities. **d**. April-May CHIRPS rainfall ranks. **e**.
566 Time series of GPCC and CHIRPS April-May rainfall for Kenya (excluding Nyanza and Western Province)
567 as south-central and south-eastern Ethiopia, as indicated by the inset map in **e**.

568 **Figure 6**. **a.** Time series of smoothed standardized GPCC for study region (red solid line)**,** and WPG-based
569 estimates of GPCC SPI (blue dashed line). **b.** The western Pacific (red solid line) and Niño 4 (solid blue
570 line) contributions to the EA SPI estimates shown in blue in panel a. Dashed red and blue lines show the
571 WP and Niño 4 contribution estimates based on the mean of a 53 member CMIP5 ensemble. **c**. observed
572 western Pacific SST anomalies (solid red line), CMIP5 western Pacific SST anomalies (dashed blue line),
573 and linear fits (straight red and blue lines). **d**. detrended western Pacific SST anomalies (solid red line)
574 and detrended CMIP5 western Pacific SST anomalies (dashed blue line).

575

576

Acknowledgements

583

<div align="center">

References

</div>

585

586 Adler, R. F., Huffman, G. J., Chang, A., Ferraro, R., Xie, P., Janowiak, J., Rudolf, B., Schneider,
587 U., Curtis, S., Bolvin, D., Gruber, A., Susskind, J., and Arkin, P.: The version 2 Global
588 Precipitation Climatology Project (GPCP) monthly precipitation analysis (1979-present), J
589 Hydrometeor, 4, 1147-1167, 2003.
590 Cook, K. H., and Vizy, E. K.: Projected Changes in East African Rainy Seasons, Journal of
591 Climate, 2013.
592 England, M. H., McGregor, S., Spence, P., Meehl, G. A., Timmermann, A., Cai, W., Gupta, A.
593 S., McPhaden, M. J., Purich, A., and Santoso, A.: Recent intensification of wind-driven
594 circulation in the Pacific and the ongoing warming hiatus, Nature Climate Change, 2014.
595 Folkins, I., and Braun, C.: Tropical rainfall and boundary layer moist entropy, Journal of climate,
596 16, 1807-1820, 2003.
597 Funk, C., Asfaw, A., Steffen, P., Senay, G. B., Rowland, J., and Verdin, J. P.: Estimating Meher
598 crop production using rainfall in the 'Long Cycle' region of Ethiopia. FEWS NET Rpecial
599 Report., 2003.
600 Funk, C., Senay, G., Asfaw, A., Verdin, J., Rowland, J., Michaelson, J., Eilerts, G., Korecha, D.,
601 and Choularton, R.: Recent drought tendencies in Ethiopia and equatorial-subtropical eastern
602 Africa, US Agency for International Development, Washington, DC, 2005.
603 Funk, C., Dettinger, M. D., Michaelsen, J. C., Verdin, J. P., Brown, M. E., Barlow, M., and
604 Hoell, A.: Warming of the Indian Ocean threatens eastern and southern African food security but
605 could be mitigated by agricultural development, Proc Nat Acad Sci USA, 105, 11081-11086,
606 2008.
607 Funk, C.: Exceptional warming in the Western Pacific-Indian Ocean Warm Pool has contributed
608 to more frequent droughts in Eastern Africa, B Am Meteorol Soc, 7, 1049-1051, 2012.
609 Funk, C., Michaelsen, J., and Marshall, M.: Mapping recent decadal climate variations in
610 precipitation and temperature across Eastern Africa and the Sahel, in: Remote Sensing of
611 Drought: Innovative Monitoring Approaches, edited by: Wardlow, B., Anderson, M., and
612 Verdin, J., CRC Press 2012, Boca Raton, Florida, USA, 25 pages, 2012.

613   Funk, C., Husak, G., Michaelsen, J., Shukla, S., Hoell, A., Lyon, B., Hoerling, M. P., Liebmann,
614   B., Zhang, T., Verdin, J., Galu, G., Eilerts, G., and Rowland, J.: Attribution of 2012 and 2003-12
615   rainfall deficits in eastern Kenya and southern Somalia, Bull. Amer. Meteor. Soc., , 94, 45-48,
616   2013.
617   Funk, C., Peterson, P., Landsfeld, M., Pedreros, D., Verdin, J., Rowland, J., Romero, B., Husak,
618   G., Michaelsen, J., and Verdin, A.: A Quasi-global Precipitation Time Series for Drought
619   Monitoring, USGS, EROS Data Center, 2014.
620   Gill, A. E.: Some simple solutions for heat-induced tropical circulation, Q J Roy Meteor Soc,
621   106, 447-462, 1980.
622   Hastenrath, S., Polzin, D., and Mutai, C.: Circulation mechanisms of Kenya rainfall anomalies,
623   Journal of Climate, 24, 404-412, 2011.
624   Hoell, A., and Funk, C.: The ENSO-Related West Pacific Sea Surface Temperature Gradient,
625   Journal of Climate, 26, 2013a.
626   Hoell, A., and Funk, C.: Indo-Pacific sea surface temperature influences on failed consecutive
627   rainy seasons over eastern Africa, Climate Dynamics, 1-16, DOI 10.1007/s00382-013-1991-6,
628   2013b.
629   Hoell, A., and Funk, C.: The forcing of March-May East Africa rainfall by the warming trend in
630   Pacific sea surface temperatures and Pacific Decadal Variability, Clim. Dyn., 2013c.
631   Hoell, A., and Funk, C.: Indo-Pacific Sea Surface Temperature Influences on Failed Consecutive
632   Rainy Seasons over Eastern Africa, Clim Dyn, in press, 2013d.
633   Hoell, A., and Funk, C.: The ENSO-related west pacific sea surface temperature gradient,
634   Journal of Climate, 2013e.
635   Hoell, A., Funk, C., and Barlow, M.: The regional forcing of Northern hemisphere drought
636   during recent warm tropical west Pacific Ocean La Niña events, Climate Dynamics, 1-23, DOI
637   10.1007/s00382-013-1799-4, 2013.
638   Indeje, M., Semazzi, F. H., and Ogallo, L. J.: ENSO signals in East African rainfall seasons,
639   International Journal of Climatology, 20, 19-46, 2000.
640   Jury, M. R.: Ethiopian decadal climate variability, Theoretical and Applied Climatology, 101,
641   29-40, 2010.
642   Jury, M. R., and Funk, C.: Climatic trends over Ethiopia: regional signals and drivers,
643   International Journal of Climatology, 33, 1924-1935, 10.1002/joc.3560, 2013.
644   L'Heureux, M. L., Lee, S., and Lyon, B.: Recent multidecadal strengthening of the Walker
645   circulation across the tropical Pacific, Nature Climate Change, 2013.
646   Liebmann, B., Hoerling, M. P., Funk, C., Bladé, I., Dole, R. M., Allured, D., Pegion, P., and
647   Eischeid, J. K.: Understanding Eastern Horn of Africa Rainfall Variability and Change, J.
648   Climate, In Review, 2013.
649   Liebmann, B., Hoerling, M. P., Funk , C., Bladé, I., Dole, R. M., Allured, D., Quan, X., Pegion,
650   P., and Eischeid, J. K.: Understanding Recent Eastern Horn of Africa Rainfall Variability and
651   Change, J. Climate, In Press, 2014.
652   Lindzen, R. S., and Nigam, S.: On the role of sea surface temperature gradients in forcing Low-
653   Level winds and convergence in the tropics, Journal of the Atmospheric Sciences, 44, 2418-
654   2436, 1987.
655   Lyon, B., and DeWitt, D. G.: A recent and abrupt decline in the East African long rains,
656   GEOPHYSICAL RESEARCH LETTERS, 39, 10.1029/2011gl050337, 2012.

Lyon, B., Barnston, A. G., and DeWitt, D. G.: Tropical pacific forcing of a 1998–1999 climate shift: observational analysis and climate model results for the boreal spring season, Climate Dynamics, 1-17, 2013.

McKee, T. B., Doesken, N. J., and Kleist, J.: The relationship of drought frequency and duration to time scales, Proceedings of the 8th Conference on Applied Climatology, Anaheim, CA, 1993, 179-183,

Meehl, G. A., Hu, A., Arblaster, J. M., Fasullo, J., and Trenberth, K. E.: Externally Forced and Internally Generated Decadal Climate Variability Associated with the Interdecadal Pacific Oscillation, Journal of Climate, 26, 2013.

Mwangi, E., Wetterhall, F., Dutra, E., Di Giuseppe, F., and Pappenberger, F.: Forecasting droughts in East Africa, Hydrol. Earth Syst. Sci., 18, 611-620, 10.5194/hess-18-611-2014, 2014.

Nicholson, S. E., and Kim, J.: The relationship of the El Nino-Southern oscillation to African rainfall, International Journal of Climatology, 17, 117-135, 1997.

Nicholson, S. E., and Selato, J. C.: The influence of La Nina on African rainfall, International Journal of Climatology, 20, 1761-1776, 2000.

Nicholson, S. E.: The Predictability of Rainfall over the Greater Horn of Africa. Part I: Prediction of Seasonal Rainfall, Journal of Hydrometeorology, 15, 1011-1027, 10.1175/JHM-D-13-062.1, 2014a.

Nicholson, S. E.: A detailed look at the recent drought situation in the Greater Horn of Africa, J Arid Environ, 103, 71-79, 2014b.

Ogallo, L. J.: Relationships between seasonal rainfall in East Africa and the Southern Oscillation, International Journal of Climatology, 8, 31-43, 10.1002/joc.3370080104, 1988.

Omondi, P. A. o., Awange, J. L., Forootan, E., Ogallo, L. A., Barakiza, R., Girmaw, G. B., Fesseha, I., Kululetera, V., Kilembe, C., and Mbati, M. M.: Changes in temperature and precipitation extremes over the Greater Horn of Africa region from 1961 to 2010, International Journal of Climatology, 2013.

Pohl, B., and Camberlin, P.: Influence of the Madden-Julian Oscillation on East African rainfall. I: Intraseasonal variability and regional dependency, Quarterly Journal of the Royal Meteorological Society, 132, 2521-2539, 2006.

Pricope, N. G., Husak, G., Lopez-Carr, D., Funk, C., and Michaelsen, J.: The climate-population nexus in the East African Horn: Emerging degradation trends in rangeland and pastoral livelihood zones, Glob Environ Change, 23, 1525-1541, 2013.

Saji, N. H., Goswami, B. N., Vinayachandran, P. N., and Yamagata, T.: A dipole mode in the tropical Indian Ocean, Nature, 401, 360-363, 1999.

Sandeep, S., Stordal, F., Sardeshmukh, P. D., and Compo, G. P.: Pacific Walker Circulation variability in coupled and uncoupled climate models, Climate Dynamics, 1-15, 2014.

Schneider, U., Becker, A., Finger, P., Meyer-Christoffer, A., Ziese, M., and Rudolf, B.: GPCC's new land surface precipitation climatology based on quality-controlled in situ data and its role in quantifying the global water cycle, Theoretical and Applied Climatology, 1-26, 10.1007/s00704-013-0860-x, 2013.

Sheffield, J., Wood, E. F., Chaney, N., Guan, K., Sadri, S., Yuan, X., Olang, L., Amani, A., Ali, A., and Demuth, S.: A Drought Monitoring and Forecasting System for Sub-Sahara African Water Resources and Food Security, B Am Meteorol Soc, http://dx.doi.org/10.1175/BAMS-D-12-00124.1, 2013.

701 Shukla, S., Sheffield, J., Wood, E., and Lettenmaier, D.: On the sources of global land surface
702 hydrologic predictability, Hydrology and Earth System Sciences Discussions, 10, 1987-2013,
703 2013.
704 Shukla, S., Funk, C., and Hoell, A.: Using constructed analogs to improve the skill of March-
705 April-May precipitation forecasts in equatorial East Africa, Environ Res Lett, In Review, 2014a.
706 Shukla, S., McNally, A., Husak, G., and Funk, C.: A seasonal agricultural drought forecast
707 system for food-insecure regions of East Africa, Hydrology and Earth System Sciences
708 Discussions, 11, 3049-3081, 2014b.
709 Smith, T. M., Reynolds, R. W., Peterson, T. C., and Lawrimore, J.: Improvements to NOAA's
710 Historical Merged Land–Ocean Surface Temperature Analysis (1880–2006), Journal of Climate,
711 21, 2283-2296, 10.1175/2007jcli2100.1, 2008.
712 Taylor, K. E., Stouffer, R. J., and Meehl, G. A.: An Overview of CMIP5 and the Experiment
713 Design, B Am Meteorol Soc, 93, 485-498, 10.1175/bams-d-11-00094.1, 2011.
714 Tierney, J., Smerdon, J., Anchukaitis, K., and Seager, R.: Multidecadal variability in East
715 African hydroclimate controlled by the Indian Ocean Peer reviewed article, Nature, 493, 389-
716 392, 2013.
717 Verdin, J., Funk, C., Senay, G., and Choularton, R.: Climate science and famine early warning,
718 Philos T Roy Soc B, 360, 2155-2168, 2005.
719 Ververs, M.-T.: The East African Food Crisis: Did Regional Early Warning Systems Function?,
720 Journal of Nutrition, 142, 131-133, 10.3945/jn.111.150342, 2011.
721 Viste, E., Korecha, D., and Sorteberg, A.: Recent drought and precipitation tendencies in
722 Ethiopia, Theoretical and Applied Climatology, 112, 535–551, DOI 10.1007/s00704-012-0746-
723 3, 2012.
724 Williams, A., Funk, C., Michaelsen, J., Rauscher, S., Robertson, I., Wils, T., Koprowski, M.,
725 Eshetu, Z., and Loader, N.: Recent summer precipitation trends in the Greater Horn of Africa and
726 the emerging role of Indian Ocean sea surface temperature, Climate Dynamics, 1-22,
727 10.1007/s00382-011-1222-y, 2011.
728 Williams, P., and Funk, C.: A westward extension of the warm pool leads to a westward
729 extension of the Walker circulation, drying eastern Africa, Climate Dynamics, DOI
730 10.1007/s00382-010-0984-y, 2011.
731 Yang, W., Seager, R., Cane, M. A., and Lyon, B.: The East African long rains in observations
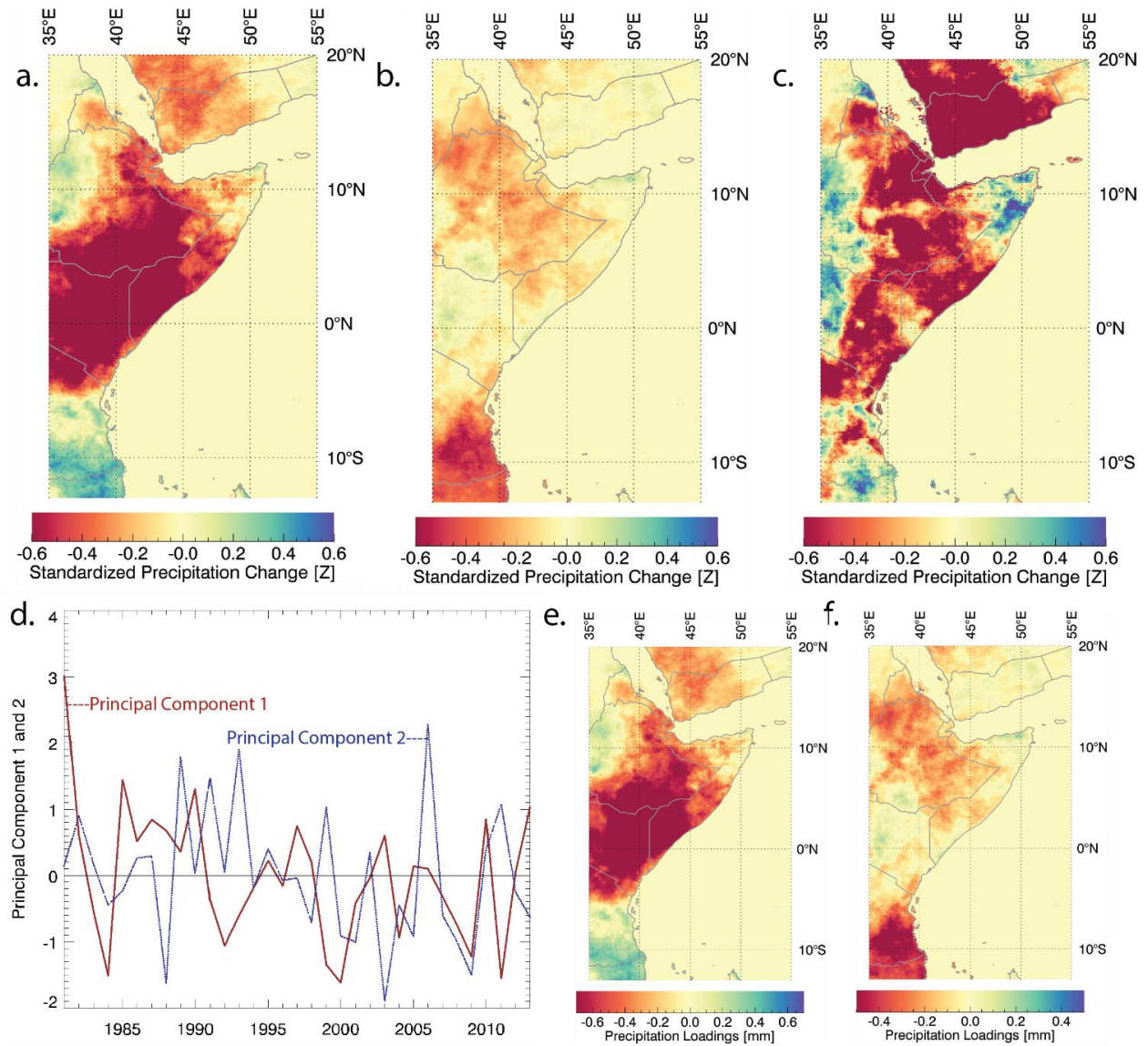732 and models, Journal of Climate, 2014.
733
734
735

736

Figure 1. **a**. Thirty-three year changes in standardized March-May precipitation associated with the trend in principal component 1 **b**. same for principal component 2. **c**. Thirty- three year changes in standardized March-May precipitation associated with a linear trend **d**. Standardized time series of PC1 (solid red line) and PC2 (dashed blue line).
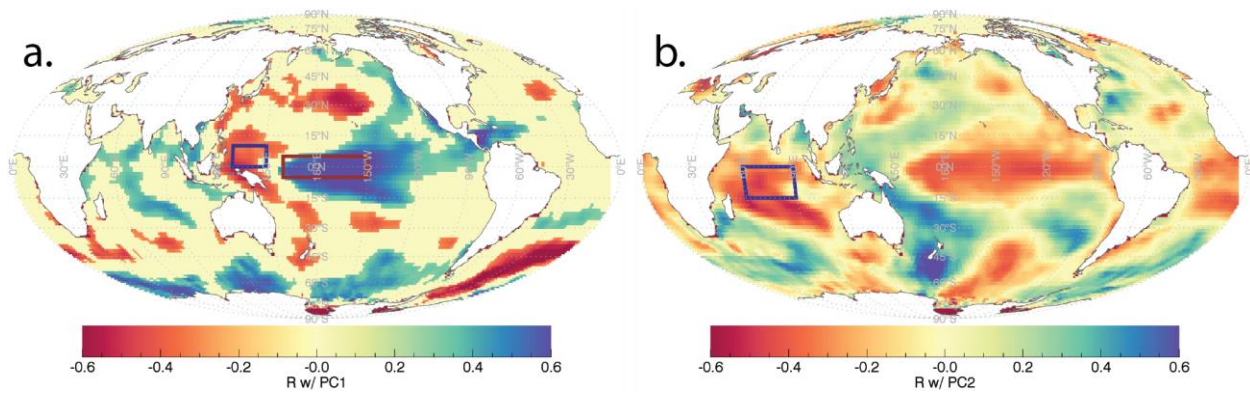
741

742

Figure 2. a. correlations between March-May CHIRPS PC1 and January SSTs **b**. same for CHIRPS PC2. Values have been screened at a 10% significance level. Boxes in panel **a** and **b** show the regions used to the define the WPG and CIO SST indices.

746

747
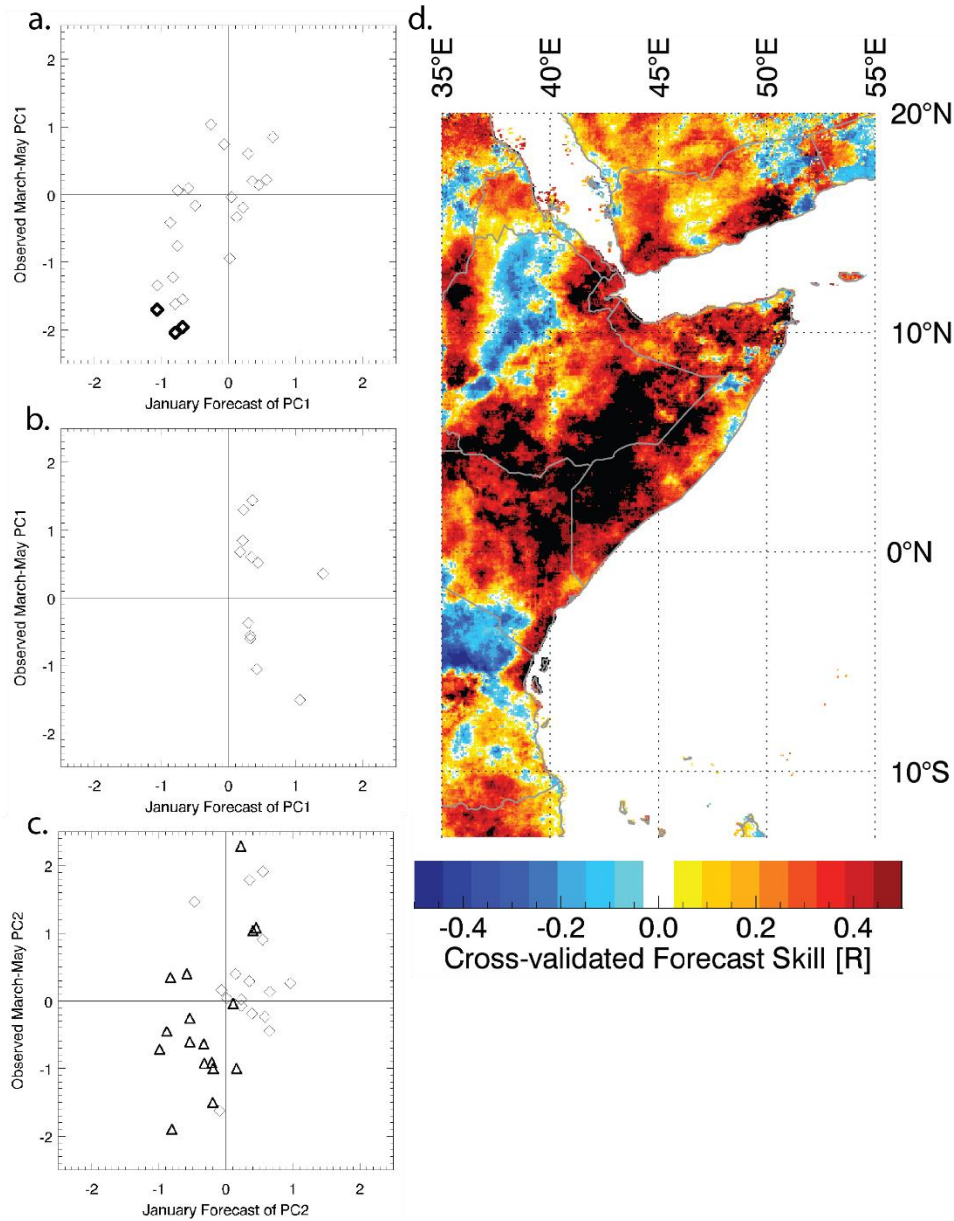
Figure 3. **a**. Scatterplot of 1994-2013 March-May PC1 observations (y axis) and cross-validated PC1
estimates based on January WPG SSTs (x axis). **b**. Same but for 1981-1993. **c**. Scatterplot of 1981-2013
March-May PC2 observations (y axis) and PC1 estimates based on January WPG SSTs (x axis). **d**. 1993-
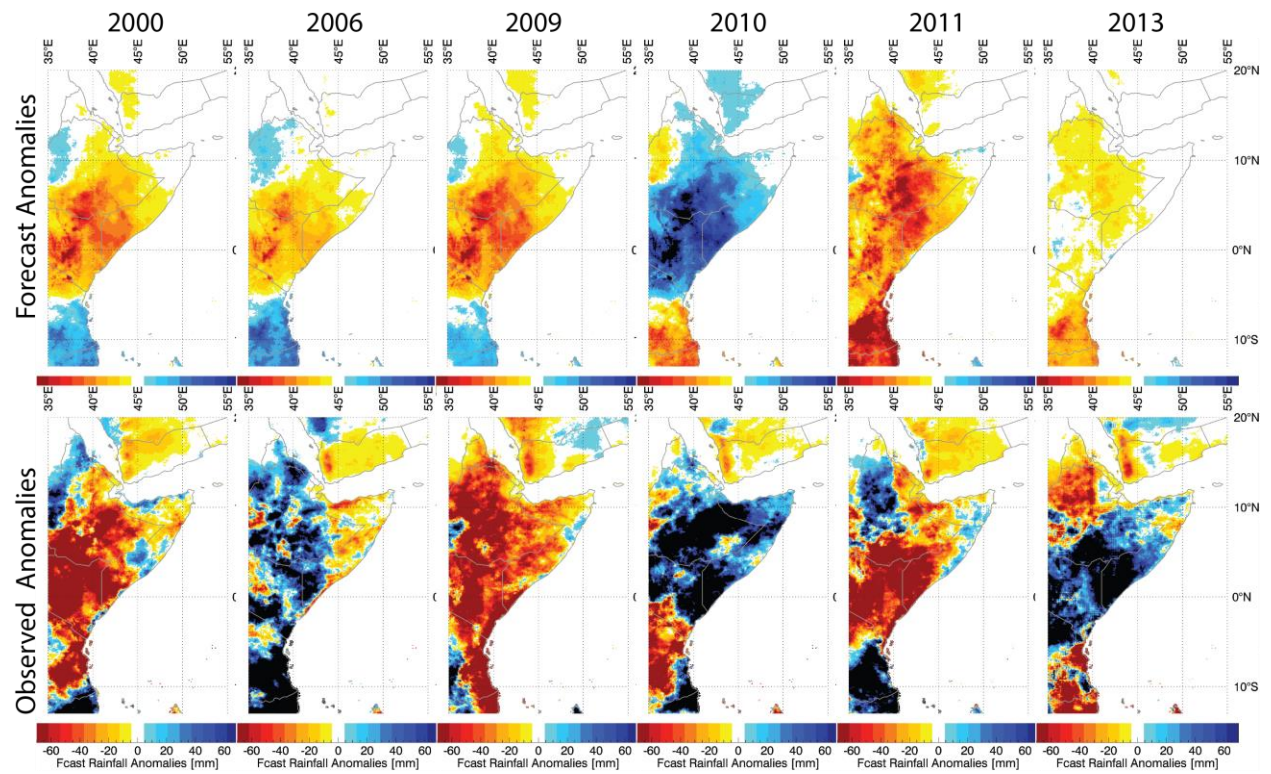2013 correlation between forecasts and observed rainfall.

752

753

Figure 4. Forecasts and observed March-May SPI values for 2000, 2006, 2009, 2010, 2011 and 2013.
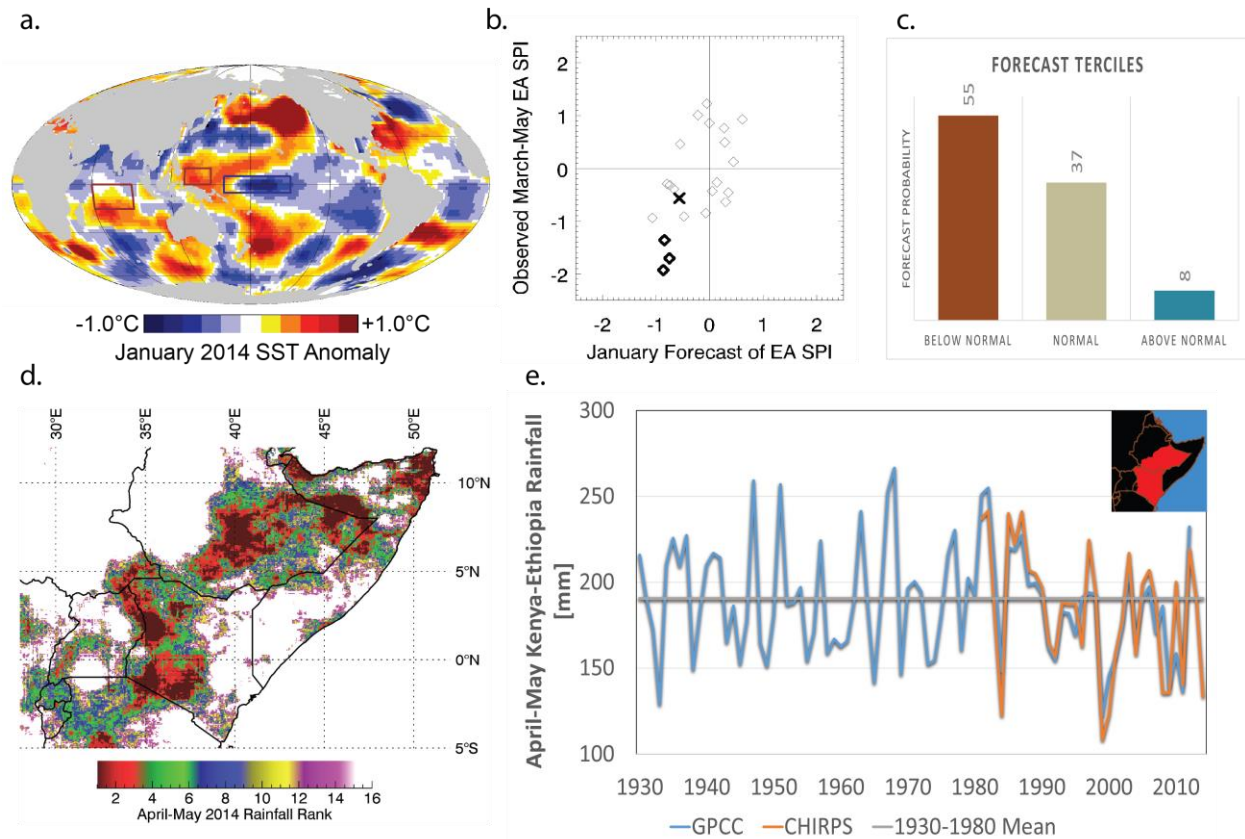
755

756

Figure 5. **a**. January 2014 SST anomalies. **b**. Scatterplot of observed and hindcast East African March-May SPI values. Bold diamonds denote 2000, 2009 and 2011. The bold X marks the forecast for 2014 made in February of 2014. **c**. Forecast rainfall tercile probabilities. **d**. April-May CHIRPS rainfall ranks. **e**. Time series of GPCC and CHIRPS April-May rainfall for Kenya (excluding Nyanza and Western Province) as south-central and south-eastern Ethiopia, as indicated by the inset map in **e**.
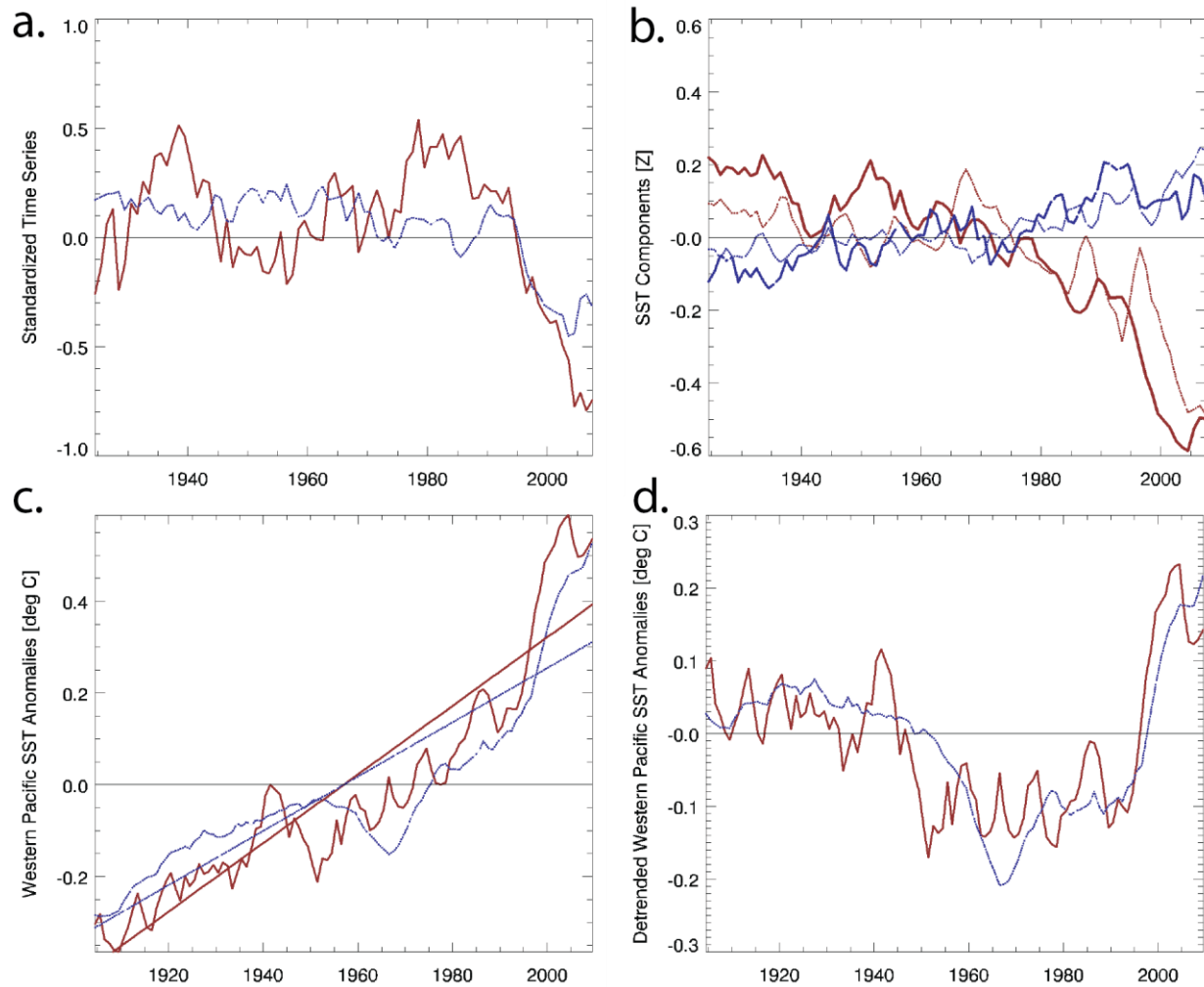
762

Figure 6. **a.** Time series of smoothed standardized GPCC for study region (red solid line)**,** and WPG-based estimates of GPCC SPI (blue dashed line). **b.** The western Pacific (red solid line) and Niño 4 (solid blue line) contributions to the EA SPI estimates shown in blue in panel a. Dashed red and blue lines show the WP and Niño 4 contribution estimates based on the mean of a 53 member CMIP5 ensemble. **c.** observed western Pacific SST anomalies (solid red line), CMIP5 western Pacific SST anomalies (dashed blue line), and linear fits (straight red and blue lines). **d.** detrended western Pacific SST anomalies (solid red line) and detrended CMIP5 western Pacific SST anomalies (dashed blue line).